Volume 1 | Number 1 | Jan 2013 | Pages 1–100

Journal of
**Materials Chemistry A**

Materials for energy and sustainability
www.rsc.org/materialsA

Li⁺

ROYAL SOCIETY
OF CHEMISTRY

This is an *Accepted Manuscript*, which has been through the Royal Society of Chemistry peer review process and has been accepted for publication.

*Accepted Manuscripts* are published online shortly after acceptance, before technical editing, formatting and proof reading. Using this free service, authors can make their results available to the community, in citable form, before we publish the edited article. We will replace this *Accepted Manuscript* with the edited and formatted *Advance Article* as soon as it is available.

You can find more information about *Accepted Manuscripts* in the **Information for Authors**.

Please note that technical editing may introduce minor changes to the text and/or graphics, which may alter content. The journal's standard **Terms & Conditions** and the **Ethical guidelines** still apply. In no event shall the Royal Society of Chemistry be held responsible for any errors or omissions in this *Accepted Manuscript* or any consequences arising from the use of any information it contains.

# Journal Name

## ARTICLE

# Template-free ultraspray pyrolysis synthesis of N/Fe-doped carbon microspheres for oxygen reduction electrocatalysis†

S. Marzorati,[a] J. M. Vasconcelos,[b] J. Ding,[b] M. Longhi,[a] and Paula E. Colavita,[b*]

Ultrasonic spray pyrolysis was used in a continuous flow apparatus for the template-free synthesis of iron- and nitrogen-doped porous carbon materials. Solutions of glucose, histidine and $Fe(CH_3COO)_2$ were nebulized and pyrolyzed yielding carbon microspheres. Scanning Electron Microscopy (SEM), Energy Dispersive Spectroscopy (EDS) and Focused Ion Beam (FIB) milling revealed that microspheres initially possess empty cores and a smooth shell. Further annealing leads to a collapse of this shell, and formation of porous microspheres with high roughness and iron-rich aggregates. X-ray Diffraction (XRD) and Photoelectron Spectroscopy (XPS) were used to investigate bulk and surface chemistry: microspheres were found to undergo graphitization; Fe and $Fe_3C$ particles form and become encapsulated within the carbon phase, while the nitrogen present in the precursor solution results in the formation of pyridinic/pyrrolic N-centers. The microspheres were tested as electrocatalysts for the oxygen reduction reaction (ORR) in acidic solution. Polarization curves using a Rotating Disk Electrode (RDE) yielded electrocatalytic behavior, and the number of exchanged electrons $n=3.7\pm0.2$ calculated from Koutecky-Levich plots suggests that direct formation of $H_2O$ is the preferred ORR mechanism. These results indicate that this synthetic approach offers a simple and scalable strategy for the preparation of electrode materials for Polymer Electrolyte Membrane Fuel Cells.

## Introduction

The development of fuel cells (FCs) is an area of extreme interest due to the opportunity these devices offer of converting small molecules into electrical power with high efficiency and via environmentally friendly processes.[1-3] Polymer electrolyte membrane FCs (PEMFCs), including direct methanol FCs, are some of the most promising FC technologies in terms of performance and potential to mitigate emissions. The use of catalysts is essential in order to carry out both the anodic and cathodic reactions in PEMFCs; the cathodic oxygen reduction reaction (ORR) is particularly sluggish and it is responsible for the majority of power losses in PEMFCs. In order to carry out ORR at practical rates it is necessary to use catalysts which, at present, are all based on Pt-group metals and alloys supported on conductive materials.[4-7] The cost associated with Pt-group catalysts is currently considered one of the most important hurdles towards mass commercialization of FCs.[8,9] Hence, commercial deployment of FCs will only be possible provided an effective low-cost substitute for these catalytic materials is found, and there is currently great interest in the discovery and optimization of

ORR electrocatalysts that can achieve good performance using non-precious metals.

Several research groups have reported that N-doped carbons and nanocarbons, often in combination with non-noble metals (e.g. Fe, Co), can display electrocatalytic behaviour in ORR.[10-14] For instance, it has been found that substitutional nitrogen at specific positions of graphene layers in well-ordered carbon nanostructures is able to promote ORR activity.[11,12] Moreover, samples containing both nitrogen and iron, have been found to be catalytically active to various extents, leading to the hypothesis that ORR catalytic activity could be related to the presence of $N_4$-Fe and $N_2$-Fe moieties on the surface.[13,14] Besides the above mentioned compositional aspects, catalyst activity also depends on structural and morphological carbon features; in particular, an optimized carbon porosity is beneficial for fast mass transport of oxygen and ORR products to and from the catalyst active sites.[15]

In this work, an ultrasonic spray pyrolysis (USP) method was developed for the synthesis of N/Fe-doped porous carbon microspheres. USP is a flow method that is intrinsically scalable without the mass- and heat-transfer problems often encountered in batch processing; it involves generating a mist of a precursor solution that is later pyrolysed in the carrier flow of an inert gas. We used solutions of low cost sugars, which had previously been shown to yield carbon particles via USP, as precursors for the carbon material, to which we added nitrogen-containing compounds and iron salts for N- and Fe-doping.[16] In previous works by Atkinson *et al.*[17] and Zhan *et al.*[18] USP methods had been used to synthesize Fe-doped

a. *Università degli Studi di Milano, Dipartimento di Chimica, Via Golgi 19, 20133 Milano, Italy.*
b. *School of Chemistry and Centre for Research on Adaptive Nanostructures and Nanodevices (CRANN), Trinity College Dublin, Dublin 2, Ireland.*
* Email: colavitp@tcd.ie.

carbon microspheres starting from sugar and salt solutions, however, thus synthesized particles did not contain N-centres, which are essential for ORR carbon catalysis. Moreover, in our synthetic process, we avoided the use of ions, such as chlorides, which are known to reduce the efficiency of catalysts and to damage the constituent materials of FCs.[19] Liu *et al.*[20] recently prepared mesoporous carbon spheres doped with N and Fe via USP and tested their performance as catalysts for ORR. Their strategy was effective, but required the use of a hard template in order to develop pores within the carbon scaffold; the template had to be removed at the end of the process prior to electrochemical testing of the materials. The USP method reported here is continuous, template-free and single-step and opens the possibility of meeting requests in terms of porosity, size and chemical composition of the obtained spheres. In the following sections we report studies of the morphology, composition and ORR catalytic performance of USP synthesized particles and discuss the potential for USP as a process for the design of Pt-free catalysts.

## Experimental

### Materials

All reactants (Glucose, histidine, Iron (II) acetate, glacial acetic acid, Nafion® (5 wt. % EtOH solution), 37% hydrochloric acid, concentrated sulfuric acid and ethanol) were purchased from Sigma Aldrich and used as received without further purification. 60% $HClO_4$ solution was from Merck.

### Particle Synthesis

The precursor solution for particle synthesis consisted of 200 mL of a solution of glucose (Glc, 0.42 M) and histidine (His, 0.042 M) in water, yielding a 10:1 Glc:His molar ratio, as in previous work.[16] Glacial acetic acid was added to the above solution in equimolar ratio to His in order to dissolve the nitrogen-containing compound; finally, iron (II) acetate was added at 0.96 wt.% Fe concentration (calculated from the total mass of Glc, His and iron acetate). Carbon microspheres were synthesized via ultraspray pyrolysis (USP) using a home-built apparatus[21] consisting of a 1.65 MHz piezoelectric crystal (APC) and a 1 m long tube furnace (Carbolite); temperature was held at 710°C and nitrogen was used as carrier gas at 3 LPM flow. Solid particles were collected as a suspension in a water-filled flask at the end of the furnace, and later filtered and washed, 3 times with water and 3 times with ethanol, using nylon membranes (0.45 μm, 25 mm, Millipore). Thus prepared particles are hereafter referred to as GH710. Particles were then annealed under nitrogen gas flow (3 LPM) according to the following protocol: 25 min at 25°C, slow heating (6°C min$^{-1}$) up to 900°C, 3 h held at 900°C and, finally, rapid cooling to 25°C under nitrogen flow. The annealed particles are hereafter referred to as GH900.

### Characterization

Scanning Electron Microscopy (SEM) was performed at an accelerating voltage of 10 keV using a Zeiss Ultra microscope equipped with an Energy Dispersive X-ray Spectroscopy (EDS) detector (Oxford Instruments). Sample cross-sections were obtained on a Zeiss Auriga dual-beam system with a Ga focused ion beam (FIB, probe at 30 kV and 240 pA) and a SEM for imaging. Raman spectra were obtained on a Raman microscope (NTEGRA Spectra NT-MDT) equipped with a CCD camera using 514 nm excitation and 1 cm$^{-1}$ spectral resolution. In order to obtain $I_D/I_G$ ratios, peaks were fitted using a combination of a Breit-Wigner-Fano and a Lorentzian peak[22] using a commercial software (Igor Pro 6.04). The Brunauer-Emmett-Teller (BET) specific surface area was obtained from the $N_2$ adsorption/desorption isotherms at 77 K using a Micromeritics Tristar II apparatus. Specific surface area and porosity distribution were evaluated by BET and BJH theories using the instrumental software (Version 1.03). Before measurements, sample powders were heat-treated at 150°C for 4 h under a $N_2$ flow to remove adsorbed and undesired species from the sample surface. X-Ray diffraction (XRD) patterns were recorded on a powder diffractometer (Philips PW3020), with Cu Kα source (λ = 1.54056 Å), 2θ range 20°-80° in 0.02° steps with 1s counting. X-ray Photoelectron Spectroscopy (XPS) measurements were performed with an M-Probe Instrument (SSI) equipped with a monochromatic Al Kα source (1486.6 eV) at an energy resolution of 0.2 eV and a take-off angle of 45°. Peaks were fitted to Voigt functions after Shirley background correction,[23] using commercial software (Igor Pro 6.04). Atomic relative percentages were obtained from peak area ratios corrected by empirical relative sensitivity factors derived by Wagner *et al.*:[24] F 1s=1, C 1s=0.25, O 1s=0.66, N 1s=0.42, Fe 2p$_{3/2}$=2. Electrochemical characterization was performed in 0.10 M $HClO_4$ solution by the Thin Film Rotating Disk Electrode method via cyclic voltammetry (CV). All glassware used for electrochemical measurements was washed with 37% HCl, rinsed with abundant water, then with concentrated $H_2SO_4$ and finally rinsed again with water. A potentiostat (AMEL 7050) with a three-electrode setup was used: a rotating disk electrode (RDE, EDI 101 Radiometer) as working electrode, an Ag/AgCl reference electrode (3 M NaCl, Amel) immersed in an external compartment connected to the cell by a capillary, and a graphite counterelectrode (Amel 201/S-016). Before RDE assembly, the tip was gently cleaned with soft sandpaper and polished with diamond powder. 10 mg of the catalyst powder were suspended in 1 mL of water; 5 μL of commercial Nafion® were added to the suspension which underwent 20 minutes of sonication; finally, 7 μL of this suspension were deposited onto the RDE glassy carbon tip (geometric surface area of 0.07 cm$^2$) and dried in a bottom-up position under a tungsten lamp (100 W). Measurements were recorded between 0.8 V and -0.275 V (vs. Ag/AgCl) at 5 mV s$^{-1}$ scan rate, at a constant temperature of 25°C. Electrochemical data for catalysts samples was obtained by following a multistep protocol. First, solutions were degassed for 20 min by bubbling $N_2$ at 5 Ndm$^3$ h$^{-1}$ and three conditioning potential cycles were acquired in this $N_2$-saturated solution. Second, solutions were saturated with $O_2$ for 20 min at 10 Ndm$^3$ h$^{-1}$ gas flow and fourteen conditioning potential cycles were acquired in this $O_2$-saturated solution.
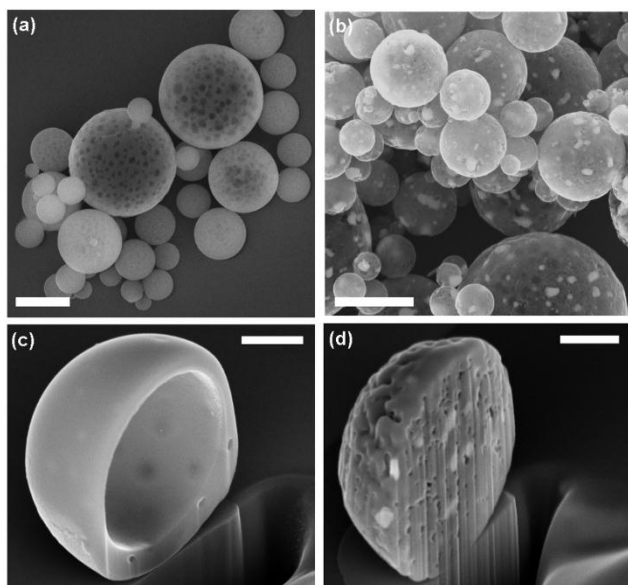
**Figure 1:** SEM images of (a) GH710 and (b) GH900 microspheres (scalebar = 1 μm). Images of typical cross sections of (c) GH710 and (d) GH900 microspheres obtained using focused Ga-ion milling (FIB) (scalebar = 400 nm).

Three potential cycles were then collected at different electrode rotation rates. To verify electrode stability and internal reproducibility three CVs at ω=1600 rpm were recorded as the first, intermediate and last measurement at this stage. Finally, the solution was degassed with $N_2$ as in the initial step, and a final measurement was recorded at 1600 rpm to obtain background faradaic currents for correcting $O_2$ reduction data.

## Results and discussion

### Characterization of carbon microspheres

Carbon microspheres were synthesized in a continuous flow apparatus via USP. A piezoelectric nebulizer placed at the bottom of a flask was used to generate a mist from the aqueous Glc: His: Fe solution; the mist was carried by a nitrogen flow into a tube furnace at 710°C yielding solid particles (GH710) that were collected as a suspension and later isolated via filtration. Dried GH710 particles were later annealed under nitrogen to obtain GH900 particles. GH710 and GH900 powders were first characterized by SEM to determine particle size and morphology. Figure 1a and 1b show SEM images of GH710 and GH900, respectively. GH710 spheres are smooth and spherical in shape; in some of the images it is also possible to discern the presence of darker spots, possibly attributable to relatively large empty cavities below the external solid shell. GH900 annealed particles retain the spherical shape of as-prepared GH710 particles, however, their surface is rougher and typically displays cracks and wide holes. Furthermore, small bright aggregates that are uniformly distributed throughout the surface of the microspheres can be clearly seen after annealing. SEM images were used to carry out particle-size analysis over 100 particles, yielding size distributions histograms (see Supporting Information). The
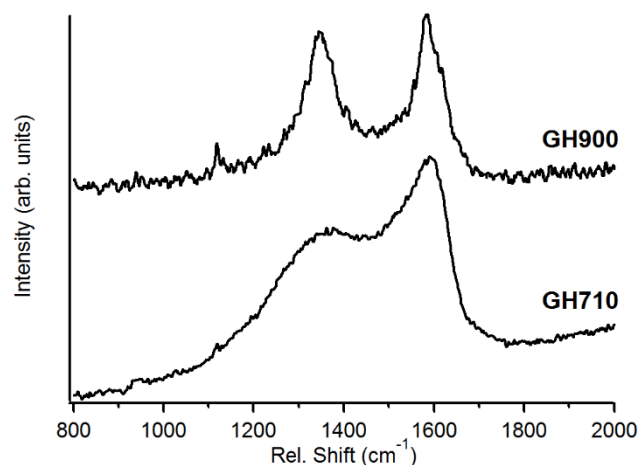


**Figure 2:** Raman spectra of GH710 and GH900 microspheres (514 nm excitation); spectra were normalized by the G peak height and offset to facilitate comparison.

average particle size was found to be 0.92 ± 0.11 μm and 0.86 ± 0.12 μm (C.I. 99%) for GH710 and GH900, respectively, suggesting no significant change in the outer diameter of particles due to annealing. The histograms are approximately log-normal in shape, yielding geometric means of 0.81 and 0.74 μm for GH710 and GH900, respectively, and geometric standard deviations of 1.64 in both cases.

The structure of synthesized and annealed particles was analyzed using FIB milling. Figures 1c and 1d show typical cross sections of GH710 and GH900 particles, respectively, obtained after exposure to a Ga-ion beam. The vast majority of GH710 particles display a hollow-shell structure, with the largest spheres often containing smaller hollow particles. Similar hollow-sphere structures were obtained by Xu *et al.* using USP methods, albeit with a different precursor solution.[25] FIB cross-sections also confirmed that darker spots visible in the SEM analysis are due to the presence of empty cavities trapped within the carbon shell. FIB cross sections of GH900 indicate that the annealing treatment not only affects the surface of the microspheres but it deeply affects the internal structure (Figure 1d). GH900 particles were all found to have a solid core containing some internal pores and bright clusters, previously observed also at the surface of GH900 by SEM; these clusters were found to be embedded in the microsphere internal volume resulting in a pudding-like structure. This pudding structure has been previously observed in the literature; Zhan *et al.*[18] synthesized iron/carbon particles via pyrolysis of sucrose solutions for applications in reductive remediation of organochlorides and reported the formation of similar bright clusters after prolonged heating, which they attributed to iron nanoparticle formation and sintering. Formation and sintering of iron oxide nanoparticles within the carbon matrix was also observed via TEM by Atkinson *et al.*[17] after USP of selected sucrose/Fe(NO$_3$)$_3$ solutions.

Figure 2 shows Raman spectra of GH710 and GH900. Both spectra show the characteristic D and G peaks of amorphous carbon materials at about 1355 and 1590 cm$^{-1}$, respectively.[22] This indicates that the Glc:His:Fe precursor solution undergoes pyrolysis during its transit in the furnace yielding particles that
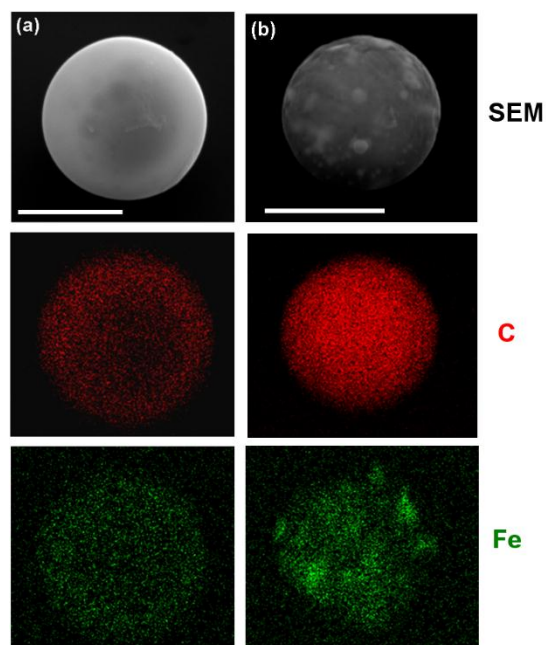
**ARTICLE**

**Figure 3:** EDS mapping of SEM images of (a) GH710 and (b) GH900 microspheres (scalebar = 1 μm); the panels show the SEM image and its corresponding C (red) and Fe (green) channels showing elemental distribution.



**Figure 4:** XRD pattern of GH900 microspheres. The reference XRD pattern of $Fe_3C$ is reported at the bottom; reflections due to the presence of α-Fe and graphite are also labeled as indicated in the legend.

contain amorphous carbon. The D peak is related to vibrations that are forbidden in perfect graphite and become active in the presence of disorder and defects; the G peak is attributed to in-plane bond-stretching vibrations of trigonally bonded carbon atoms ($sp^2$ centers).[26, 27] Upon annealing, both D and G peaks become narrower and the intensity of the D peak increases relative to that of the G peak: peak fitting yielded an increase in $I_D/I_G$ peak height ratio from 0.66 to 0.90 for GH710 and GH900, respectively. An increase in the number and size of graphitic clusters is known to translate into an increase in $I_D/I_G$ in amorphous carbons, according to the three-stage model of Ferrari *et al.*[22] Therefore, our results indicate that the annealing step leads to graphitization of the amorphous carbon phase in the particles.

In order to better understand changes in surface morphology observed after annealing, we carried out $N_2$ adsorption/desorption measurements and BET analysis. $N_2$ adsorption/desorption isotherms at 77 K of GH710 and GH900 are reported in the Supporting Information. Based on IUPAC classification, GH710 yields II-type adsorption isotherm, typical of non-porous or macroporous solids;[28] the desorption branch does not display any evident hysteresis, thus excluding the presence of a porous structure. The BET surface area of GH710 samples was found indeed to be very low, equal to 16.4 ± 0.9 $m^2$ $g^{-1}$, and consistent with the smooth appearance of microspheres observed via SEM (Figure 1a and 1c). Interestingly, the BET surface area value of GH710 is only slightly higher than the theoretical surface area of 10 $m^2$ $g^{-1}$, calculated for smooth perfect carbon spheres of 0.8 μm diameter (2.26 g $cm^{-3}$ density[29]) and 0.1 μm wall thickness. The adsorption and desorption branches of GH900 isotherms display a hysteresis loop, often associated with slit-shaped pores on the basis of De Boer's classification (Type B
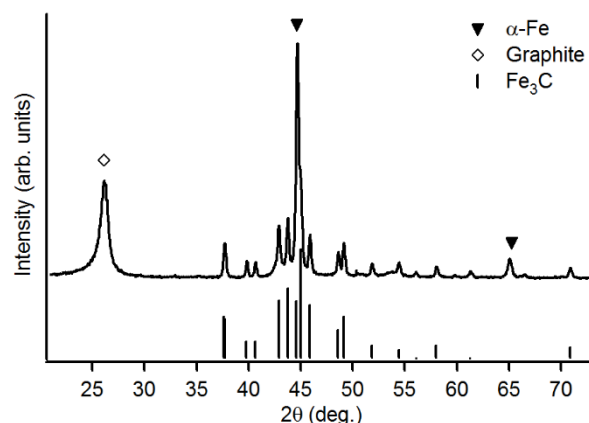
hysteresis).[30] The BET surface area of GH900 was found to be 279 ± 3 $m^2$ $g^{-1}$, a value that is 17 times higher than that of GH710 particles and comparable to that of other carbon materials suitable as electrocatalyst supports.[31] These results indicate that microspheres develop a pore structure upon annealing; this is consistent with the rough surface observed via SEM and with the observation of a solid core via FIB, which could develop without a significant decrease in microsphere diameter only if accompanied by an increase in porosity.

EDS mapping was carried out in order to investigate the elemental distribution of C and Fe. Figures 3a and 3b show EDS images of GH710 and GH900 obtained by selecting the C and Fe channels. In the case of the C channel, a completely homogeneous distribution is observed both on GH710 and GH900. In the case of the Fe channel, its distribution is homogeneous in GH710 microspheres but it is clearly concentrated in the white aggregates in GH900 microspheres. This result demonstrates that the annealing treatment not only alters the degree of graphitization of the carbon phase of synthesized particles, but it also affects the distribution of Fe, leading to the formation of Fe-rich aggregates.

The XRD pattern of GH900 microspheres is reported in Figure 4. The peaks at 2θ = 44.7° and 65.0° are assigned to the (110) and (200) reflections of α-Fe, respectively (PDF#00-006-0696); the peak at 26.4° is assigned to the (002) reflection of graphite (PDF#00-041-1487); the remaining peaks compare well to those of the iron carbide ($Fe_3C$) pattern (PDF#00-035-0772). The XRD pattern of GH900 is consistent with the majority of the iron being present in metallic or carbide forms. The formation of $Fe^0$ and $Fe_3C$ is often observed after pyrolysis of organic compounds in the presence of iron salts and are the result of carbothermal reduction and thermal decomposition of iron oxides.[18, 32-34] The carbon phase undergoes graphitization, as indicated by the appearance of a strong reflection characteristic of graphite. This is in agreement with our Raman results and is consistent with the role played by iron in catalyzing graphitization at relatively low temperatures.[35] GH710 microspheres did not yield diffraction peaks but only a broad background (data not shown), thus indicating that GH710 possess an amorphous structure.
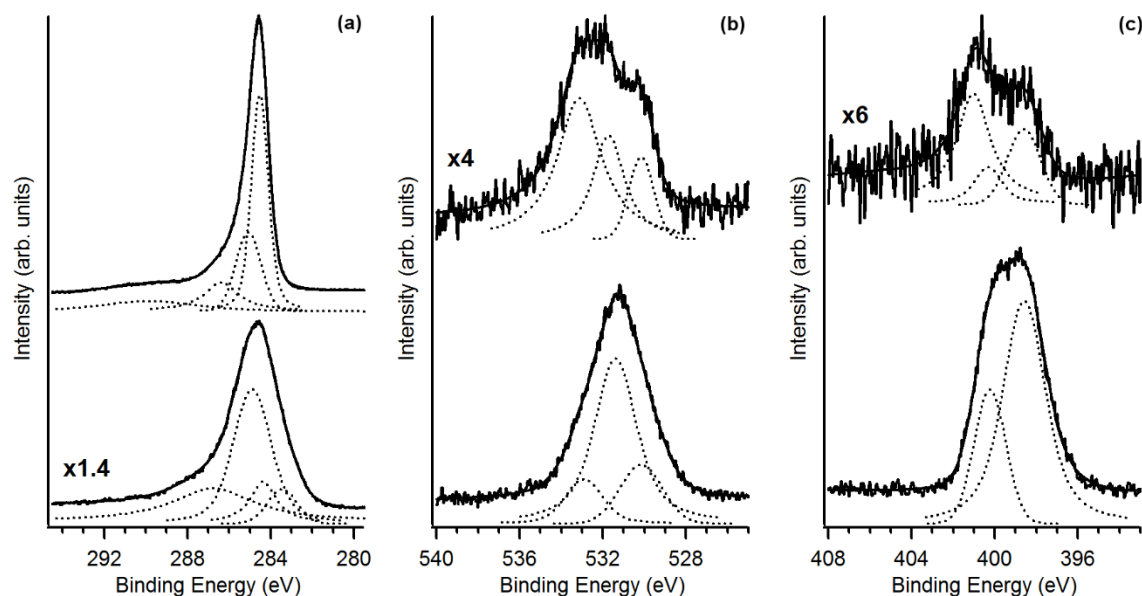
**Figure 5:** XPS spectra in the C 1s (a), O 1s (b) and N 1s (c) binding energy regions of GH710 (bottom) and GH900 (top) samples; peak contributions obtained from best fits are shown below each spectrum. Spectra are shown normalized by the C 1s total area and scaled, as indicated in each figure, to facilitate comparison.

The surface chemical species were investigated by XPS: C, O, N and Fe were detected and atomic percent results calculated relative to carbon (% O/C, % N/C and % Fe/C), as reported in Table 1; main results are reported in Figure 5. The C 1s High Resolution spectra, shown in Figure 5a for GH710 (bottom) and GH900 (top), show that the annealing process leads to a remarkable reduction in peak width. The C 1s spectrum of GH710 was deconvoluted into four contributions at 283.4 eV, assigned to carbides,[36] at 284.4 eV, assigned to graphitic carbon ($sp^2$ centres), at 284.9 eV, assigned to aliphatic carbon ($sp^3$ centres) and, finally, a broad peak at 286.8 eV, assigned to a convolution of nitrogen- and oxygen-bonded C atoms;[37, 38] further resolution of this broad peak is difficult due to fit correlations. The C 1s spectrum of GH900 was satisfactorily fitted with 4 peaks at 284.5 eV, 285.1 eV, 286.4 eV and 289.9 eV, that we attribute to $sp^2$ centres, $sp^3$ centres, C-O/C-N bonded carbon and the carbon satellite characteristic of $sp^2$-rich carbons, respectively.[37, 38] The peak area ratio $A_{284.5}/A_{285}$ increases from 0.3 for GH710 up to 2.1 for the annealed GH900 sample, further confirming that the sample undergoes significant graphitization.[39]

**Table 1.** Atomic ratios calculated relative to the C 1s line from high resolution XPS spectra for GH710 and GH900 microspheres.

| | Sample | |
| --- | --- | --- |
| | GH710 | GH900 |
| O/C% | 14 | 5.1 |
| N/C% | 32 | 3.5 |
| Fe/C% | 2.1 | 1.2 |

In Figure 5b a fit of the High Resolution O 1s region of GH710 indicates the presence of three contributions at 530.1 eV, 531.4 eV and 532.9 eV, that can be assigned to O atoms in C=O, iron hydroxides and C—O groups.[37, 40] After annealing, the O/C ratio decreases from 14% to 5.1%; three contributions can still be identified albeit with lower intensities, while the peak associated to iron hydroxide species undergoes the most significant reduction, as shown in the fit of the O 1s spectrum of GH900 (Figure 5b).[37] These results indicate that oxidized groups are lost during the annealing step; this is consistent with the graphitization process of the carbon scaffold, which typically leads to oxygen elimination in the gas phase. The significant reduction of the peak at 531.4 eV also indicates that the surface concentration of metal oxide/hydroxides decreases, in agreement with known thermal decomposition reactions of iron oxides in the presence of carbon.[32, 33]

The N 1s region of GH710 displays a strong peak that was deconvoluted into two contributions at 398.6 and 400.2 eV, characteristic of pyridinic and pyrrolic nitrogen (see Figure 5c),[41] with the former being more intense than the latter. After annealing, the nitrogen content decreases dramatically and the N 1s line develops two maxima at 398.7 eV, assigned to pyridine-type N-centres, and at 400.9 eV, that typically arises due to a convolution of pyrrolic and quaternary nitrogen at 400 and 401 eV, respectively.[42] The best fit was obtained with three peaks at 398.6 eV, 400.3 eV and 401.0 eV, as shown in Figure 5c (top); however, fit correlations make it difficult to estimate the relative proportion of pyrrolic vs. quaternary nitrogen. Similarly, we cannot exclude the possibility of contributions from iron-associated pyridinic nitrogen, which would yield a peak at 399 eV convoluted under the low binding energy maximum.[43] The $A_{398}/A_{TOT}$ ratio decreases from 74% for GH710, to 27% for GH900, thus suggesting that the proportion of pyridinic nitrogen decreases upon annealing in favor of

pyrrolic/quaternary nitrogen, in agreement with previous observations from several groups.[16, 44] Finally, iron was also detected in both GH710 and GH900 XPS spectra. The integrated area of the Fe $2p_{3/2}$ peak (See Supporting Information) was used to calculate Fe/C atomic ratios (Table 1) which were found to decrease upon annealing. This decrease is consistent both with the sintering of iron clusters and with the carbon phase having undergone graphitization, a process catalyzed by Fe/Fe$_3$C that typically leads to iron and its carbide to be encapsulated within a graphite a shell.[45, 46]

In summary, our results indicate that nebulized Glc:His:Fe solutions undergo pyrolysis yielding carbon microspheres. The annealing process results both in graphitization and phase segregation of iron-rich phases as shown by Raman and EDS. XRD results, specifically, show that metallic iron and Fe$_3$C are formed during the annealing process, whereas XPS suggests that a significant proportion of iron centers disappear into the subsurface. Interestingly, the process of annealing and graphitization also results in the development of pores. It is known from literature that iron plays an important role in carbon particle growth, acting as a Lewis acid catalyst both in the formation of carbon products and in the annealing treatment.[17, 18, 47] The transition from a hollow spherical structure, left from water evaporation in the furnace, to solid microspheres might be explain by considering that, during the annealing treatment at 900°C, the O- and N-rich carbon network is partially unstable and decomposes. This process is accompanied by the slow aggregation of dispersed iron into nanoparticles, which might serve as seeds for the catalytic "re-growth" of solid carbon spheres,[18] in a process similar to the catalytic deposition of carbon nanotubes.[48] Also, the annealing treatment leads to formation of decomposition gases which can template pores thus increasing surface area. Both the catalytic re-growth process and gas evolution within the particles could account for the presence of cracks, holes and eroded areas on GH900 observed from SEM images and the increase in BET surface area. A more detailed understanding of the mechanism of pore development is however challenging, as is often highlighted in the literature on the pyrolysis of organic compounds; mechanistic understanding would require detailed analysis of decomposition products as a function of temperature and reaction conditions as previously reported by other groups.[49-52]

### Electrochemical characterization of carbon microspheres

Electrochemical characterization was carried out in order to understand the electrocatalytic properties of GH710 and GH900 in the oxygen reduction reaction. Figure 6a compares cathodic polarization curves for ORR recorded at $\omega$ = 1600 rpm in 0.10 M HClO$_4$; current densities were normalized by BET surface areas. The GH710 sample displays poor catalytic behavior for ORR: the limiting current is undetectable and the onset potential (E$_{on}$), as calculated by the tangent method, is about -0.150 V (vs. Ag/AgCl). This potential is 0.750 V more cathodic than that observed for a commercial Pt catalyst (E$_{on}$~0.6 V vs. Ag/AgCl[16]). Figure 6a also shows the polarization curve of GH900 microspheres; the annealing treatment at
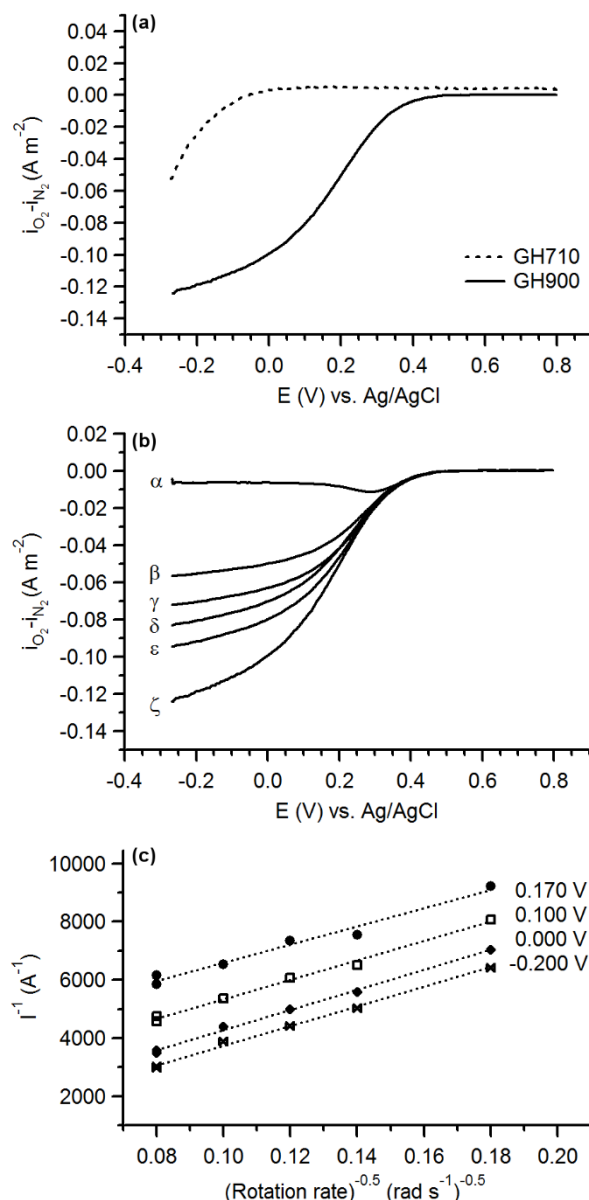


**Figure 6:** ORR Polarization Curves recorded in oxygen saturated 0.10 M HClO$_4$. T = 25 °C; (a) RDE voltammetry curves (v= 5 mV s$^{-1}$; $\omega$= 1600 rpm); (b) RDE voltammetry curves for GH900 (v = 5 mV s$^{-1}$) at $\omega$= 0 ($\alpha$), 300 ($\beta$), 500 $\gamma$), 700 ($\delta$), 900 ($\epsilon$), 1600 ($\zeta$) rpm. (c) Koutecky–Levich plots for oxygen reduction on GH900.

900°C shifts the onset potential to E$_{on}$= 0.400 V, a significant shift of 550 mV. The E$_{on}$ value is more cathodic than commercial Pt catalysts by 0.200 V, and it compares well to other Pt-free carbon based catalysts.[16] Therefore, the annealing process drastically improves the catalytic properties of microspheres in ORR.

Figure 6b shows the cathodic ORR polarization curves recorded on GH900 samples at different RDE rotation rates. A limiting current dependent on the RDE rotation rate, although not well-defined, is detectable. Figure 6c shows the corresponding Koutecky–Levich plots at different potentials.[53] The average plot slopes display good linearity and yield a number of exchanged electrons $n$ = 3.7 ± 0.2. This result indicates that peroxide formation is not the rate determining step in the reduction process and that the direct formation of H$_2$O is the

preferred ORR mechanism. Thus, the GH900 sample shows a good performance in the reduction of oxygen and can be considered a promising catalyst.

It is interesting to discuss the results of the electrochemical characterization in the context of the structural and morphological characterization of the microspheres. It has been reported in the literature that the presence of pyridinic[42, 54-57] and/or quaternary nitrogen[58, 59] surface groups enhances the ORR activity of carbon electrodes. Based on XPS and ORR results, however, GH710 displays poor ORR kinetics even though it displays a higher surface density of pyridinic sites than GH900. However, particles synthesized at 710 °C are less graphitic with presumably lower conductivity; furthermore, as suggested by previous work, the annealing treatment stabilizes N- and Fe- doped graphitic structures, increases quaternary nitrogen amount, and has been shown to activate catalytic sites for ORR.[60] However, it is difficult to determine the independent roles of N and Fe doping for promoting ORR activity: first, N-doping alone has been shown to promote ORR in carbon materials,[16, 61] second, Fe-doping is known to promote graphitization and improve carbon conductivity[18, 32-34] and finally, presence of N-complexed Fe centres is known to catalyse ORR.[14] All of the above are potential routes for ORR in our materials and further studies are necessary in order to establish a preferred mechanism. It is also important to consider the effect that annealing has on particle morphology, since BET results show that this process leads to pore opening and an increase in accessible surface sites. Therefore, the enhanced performances of GH900 microspheres vs. GH710 is likely to arise from its higher degree of graphitization, the presence of stable and active surface bound catalytic centers, and an increased availability of ORR active sites within their porous structure.

## Conclusions

In conclusion, in this work we developed a scalable, facile, template-free and rapid synthesis, of Fe- and N-doped C-based microspheres via USP. Annealing of thus synthesized materials results in the formation of graphitic microspheres containing Fe/Fe$_3$C clusters embedded in a porous carbon phase. These particles were investigated as non-noble-metal catalytic electrode materials: RDE measurements show that indeed these particles catalyse ORR and could therefore be promising as electrode materials in FCs. The surface physico-chemical characterization showed that the enhancement in ORR performances might be related to the higher degree of graphitization, the stabilization of ORR N- and/or Fe-containing active catalytic sites and the increase in surface area that result from the annealing treatment.

This work demonstrates the potential of USP methods for the synthesis of electrode materials with applications in FC technologies. Catalytic materials with relatively narrow size dispersion were prepared using low cost materials and in the absence of a templating agent. The inherent scalability of continuous flow methods such as USP represents a significant advantage compared to alternative synthetic strategies requiring batch processing or surface catalyzed deposition of nanostructured carbon materials (e.g. CVD growth). Further optimization of the catalytic performance of these materials could be achieved by investigating the use of alternative N and Fe dopant compounds in order to control the type of active sites created at the carbon scaffold surface and potentially reduce the overall cost of precursor solutions. Similarly, improved performance could be attained by controlling the size dispersion of nebulized solutions in order to improve electrode packing and, consequently, mass transport for FC applications.

## Acknowledgements

## References

1. In *Handbook of Fuel Cells: Fundamentals, Technology, Applications*, eds. W. Vielstich, A. Lamm and H. A. Gasteiger, John Wiley & Sons, Ltd, Chichester, Editon edn., 2003, vol. 3.

2. L. Carrette, K. A. Friedrich and U. Stimming, *Fuel Cells*, 2001, **1**, 5-39.

3. S. Litster and G. McLean, *J. Power Sources*, 2004, **130**, 61-76.

4. H. A. Gasteiger, S. S. Kocha, B. Sompalli and F. T. Wagner, *Appl. Catal., B*, 2005, **56**, 9-35.

5. T. Ghosh, M. B. Vukmirovic, F. J. DiSalvo and R. R. Adzic, *J. Am. Chem. Soc.*, 2009, **132**, 906-907.

6. M. Oezaslan, F. Hasché and P. Strasser, *J. Phys. Chem. Lett.*, 2013, **4**, 3273-3291.

7. A. Rabis, P. Rodriguez and T. J. Schmidt, *ACS Catalysis*, 2012, **2**, 864-890.

8. M. D. Gerst and T. E. Graedel, *Environ. Sci. Technol.*, 2008, **42**, 7038-7045.

9. C. Sealy, *Materials Today*, 2008, **11**, 65-68.

10. F. Jaouen, J. Herranz, M. Lefèvre, J.-P. Dodelet, U. I. Kramm, I. Herrmann, P. Bogdanoff, J. Maruyama, T. Nagaoka, A. Garsuch, J. R. Dahn, T. Olson, S. Pylypenko, P. Atanassov and E. A. Ustinov, *ACS Appl. Mater. Interfaces*, 2009, **1**, 1623-1639.

11. P. H. Matter, E. Wang and U. S. Ozkan, *J. Catal.*, 2006, **243**, 395-403.

12. G. Wu and P. Zelenay, *Acc. Chem. Res.*, 2013, **46**, 1878-1889.

13. M. Lefèvre, E. Proietti, F. Jaouen and J.-P. Dodelet, *Science*, 2009, **324**, 71-74.

14. N. Ramaswamy, U. Tylus, Q. Jia and S. Mukerjee, *J. Am. Chem. Soc.*, 2013, **135**, 15443-15449.

ARTICLE

15. A. Serov, M. H. Robson, M. Smolnik and P. Atanassov, *Electrochim. Acta*, 2013, **109**, 433-439.

16. I. Galbiati, C. L. Bianchi, M. Longhi, A. Carrà and L. Formaro, *Fuel Cells*, 2010, **10**, 251-258.

17. J. D. Atkinson, M. E. Fortunato, S. A. Dastgheib, M. Rostam-Abadi, M. J. Rood and K. S. Suslick, *Carbon*, 2011, **49**, 587-598.

18. J. Zhan, B. Sunkara, J. Tang, Y. Wang, J. He, G. L. McPherson and V. T. John, *Ind. Eng. Chem. Res.*, 2011, **50**, 13021-13029.

19. T. J. Schmidt, U. A. Paulus, H. A. Gasteiger and R. J. Behm, *J. Electroanal. Chem.*, 2001, **508**, 41-47.

20. H. Liu, Z. Shi, J. Zhang, L. Zhang and J. Zhang, *J. Mater. Chem.*, 2009, **19**, 468-470.

21. P. Duffy, L. M. Magno, R. B. Yadav, S. K. Roberts, A. D. Ward, S. W. Botchway, P. E. Colavita and S. J. Quinn, *J. Mater. Chem.*, 2012, **22**, 432-439.

22. A. C. Ferrari and J. Robertson, *Phys. Rev. B*, 2000, **61**, 14095-14107.

23. A. Proctor and P. M. A. Sherwood, *Anal. Chem.*, 1982, **54**, 13-19.

24. C. D. Wagner, L. E. Davis, M. V. Zeller, J. A. Taylor, R. H. Raymond and L. H. Gale, *Surf. Interface Anal.*, 1981, **3**, 211-225.

25. H. Xu, J. Guo and K. S. Suslick, *Adv. Mater.*, 2012, **24**, 6028-6033.

26. A. C. Ferrari and J. Robertson, *Phil. Trans. R. Soc. Lond. A*, 2004, **362**, 2477-2512.

27. J. H. Lehman, M. Terrones, E. Mansfield, K. E. Hurst and V. Meunier, *Carbon*, 2011, **49**, 2581-2602.

28. K. S. W. Sing, *Pure Appl. Chem.*, 1985, **57**, 603.

29. H. O. Pierson, *Handbook of Carbon, Graphite, Diamond and Fullerenes - Properties, Processing and Applications* 1st edn., Noyes Publications, Park Ridge, New Jersey, 1993.

30. S. Lowell and J. E. Shields, in *Powder Surface Area and Porosity*, Chapman & Hall, London, New York, Tokyo, Melbourne, Madras, Editon edn., 1991, p. 57.

31. P. Stonehart and D. Wheeler, in *Modern Aspects of Electrochemistry, Number 38*, ed. B. E. Conway, Springer, Editon edn., 2005, vol. 38, p. 407.

32. M. Hermanek, R. Zboril, M. Mashlan, L. Machala and O. Schneeweiss, *J. Mater. Chem.*, 2006, **16**, 1273-1280.

33. S. A. Steiner, T. F. Baumann, J. Kong, J. H. Satcher and M. S. Dresselhaus, *Langmuir*, 2007, **23**, 5161-5166.

34. J. N. Wang, L. Zhang, F. Yu and Z. M. Sheng, *J. Phys. Chem. B*, 2007, **111**, 2119-2124.

35. A. Ōya and H. Marsh, *J. Mater. Sci.*, 1982, **17**, 309-322.

36. E. Papastavros, P. J. Shea and M. A. Langell, *Langmuir*, 2004, **20**, 11509-11516.

37. S. Biniak, G. Szymański, J. Siedlewski and A. Świtkowski, *Carbon*, 1997, **35**, 1799-1810.

38. S. T. Jackson and R. G. Nuzzo, *Appl. Surf. Sci.*, 1995, **90**, 195-203.

39. J. Díaz, G. Paolicelli, S. Ferrer and F. Comin, *Phys. Rev. B*, 1996, **54**, 8064-8069.

40. M. C. Biesinger, B. P. Payne, A. P. Grosvenor, L. W. M. Lau, A. R. Gerson and R. S. C. Smart, *Appl. Surf. Sci.*, 2011, **257**, 2717-2730.

41. S. Maldonado, S. Morin and K. J. Stevenson, *Carbon*, 2006, **44**, 1429-1437.

42. S. Maldonado and K. J. Stevenson, *J. Phys. Chem. B*, 2005, **109**, 4707-4716.

43. R. Kothandaraman, V. Nallathambi, K. Artyushkova and S. C. Barton, *Appl. Catal., B*, 2009, **92**, 209-216.

44. C. Galeano, J. C. Meier, M. Soorholtz, H. Bongard, C. Baldizzone, K. J. J. Mayrhofer and F. Schüth, *ACS Catalysis*, 2014, **4**, 3856-3868.

45. C. Emmenegger, J. M. Bonard, P. Mauron, P. Sudan, A. Lepora, B. Grobety, A. Züttel and L. Schlapbach, *Carbon*, 2003, **41**, 539-547.

46. J. Geng, D. A. Jefferson and B. F. G. Johnson, *Chem. Commun.*, 2004, 2442-2443.

47. Q. Yan, C. Wan, J. Liu, J. Gao, F. Yu, J. Zhang and Z. Cai, *Green Chem.*, 2013, **15**, 1631-1640.

48. B. C. Liu, S. C. Lyu, S. I. Jung, H. K. Kang, C. W. Yang, J. W. Park, C. Y. Park and C. J. Lee, *Chem. Phys. Lett.*, 2004, **383**, 104-108.

49. A. Singh, J. Jayaram, M. Madou and S. Akbar, *J. Electrochem. Soc.*, 2002, **149**, E78-E83.

50. M. Kiyono, P. J. Williams and W. J. Koros, *J. Membr. Sci.*, 2010, **359**, 2-10.

51. S. M. Saufi and A. F. Ismail, *Carbon*, 2004, **42**, 241-259.

52. V. C. Geiszler and W. J. Koros, *Ind. Eng. Chem. Res.*, 1996, **35**, 2999-3003.

53. A. J. Bard and L. R. Faulkner, in *Electrochemical Methods: Fundamentals and Applications*, Wiley, Editon edn., 2001, pp. 331-367.

54. R. Bresciani, S. Marzorati, A. Lascialfari, B. Sacchi, N. Santo and M. Longhi, *Electrochem. Commun.*, 2015, **51**, 27-32.

55. L. Lai, J. R. Potts, D. Zhan, L. Wang, C. K. Poh, C. Tang, H. Gong, Z. Shen, J. Lin and R. S. Ruoff, *Energy Environ. Sci.*, 2012, **5**, 7936-7942.

56. S. M. Unni, S. N. Bhange, R. Illathvalappil, N. Mutneja, K. R. Patil and S. Kurungot, *Small*, 2015, **11**, 352-360.

57. D. Zhou, L. Yang, L. Yu, J. Kong, X. Yao, W. Liu, Z. Xu and X. Lu, *Nanoscale*, 2015, **7**, 1501-1509.

58. R. A. Sidik, A. B. Anderson, N. P. Subramanian, S. P. Kumaraguru and B. N. Popov, *J. Phys. Chem. B*, 2006, **110**, 1787-1793.

59. N. P. Subramanian, X. Li, V. Nallathambi, S. P. Kumaraguru, H. Colon-Mercado, G. Wu, J.-W. Lee and B. N. Popov, *J. Power Sources*, 2009, **188**, 38-44.

60. F. Jaouen, in *Non-Noble Metal Fuel Cell Catalysts*, eds. Z. Chen, J.-P. Dodelet and J. Zhang, Wiley-VCH Verlag GmbH & Co. KGaA, Weinheim, Germany, Editon edn., 2014, pp. 29-118.

61. S. Chen, J. Bi, Y. Zhao, L. Yang, C. Zhang, Y. Ma, Q. Wu, X. Wang and Z. Hu, *Adv. Mater.*, 2012, **24**, 5593-5597.
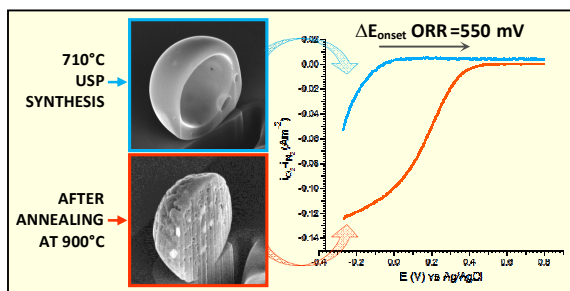
Starting from low-cost materials and no need for nanostructured templates, C-microspheres with N/Fe active sites for ORR were synthesized via a continuous-flow and scalable USP method.